PAPER

Excimer laser ablation of aluminum: influence of spot size on ablation rate

IOP Publishing | Astro Ltd Laser Physics

Laser Phys. **26** (2016) 116102 (8pp) doi:10.1088/1054-660X/26/11/116102

Excimer laser ablation of aluminum: influence of spot size on ablation rate

M E Shaheen[1], J E Gagnon[2,3] and B J Fryer[2,3]

[1] Department of Physics, Faculty of Sciences, Tanta University, Tanta, Egypt
[2] Great Lakes Institute for Environmental Research (GLIER), University of Windsor, Windsor, Ontario, N9B 3P4, Canada
[3] Department of Earth and Environmental Sciences, University of Windsor, Windsor, Ontario, N9B 3P4, Canada

E-mail: mshaheen73@science.tanta.edu.eg or mshaheen73@yahoo.com

Received 29 August 2016, revised 6 September 2016
Accepted for publication 6 September 2016
Published 30 September 2016

Abstract

The dependence of ablation rate of an Al alloy on laser beam spot size (10–150 μm) was investigated using an ArF excimer laser operating at a wavelength of 193 nm and pulse width less than 4 ns. Ablation was conducted in air at a fluence of 11 J cm^{-2} and at a repetition rate of 20 Hz. Surface morphology and depth of craters produced by a variable number of laser pulses were characterized using optical and scanning electron microscopy. Laser ablation inductively coupled plasma mass spectrometry (LA-ICP-MS) was used as an additional diagnostic technique to estimate the amount of material ablated from craters produced by a laser beam of different diameters. Laser beam spot size and number of laser pulses applied to the same spot were found to influence crater morphology, ablation rate, shape and amount of particles deposited at or around the crater rim. Ablation rate was found to be less dependent on spot size for craters greater than 85 μm. A four-fold increase in ablation rate was observed with decreasing crater size from 150 μm to 10 μm.

Keywords: excimer laser, aluminum, SEM, ablation rate, surface morphology

(Some figures may appear in colour only in the online journal)

1. Introduction

Excimer lasers are widely used in many applications, such as chemical analysis of solid samples by laser ablation inductively coupled plasma mass spectrometry (LA-ICP-MS) [1–3], high-resolution photolithography, which is a critical technology used in the manufacturing of microelectronic devices [4, 5], micromachining and processing of a wide range of materials [5–10], and many other applications [11–14]. The fast growth in excimer laser applications over the last two decades is largely related to the availability of relatively low cost, reliable, and powerful commercial laser systems, together with the need for better understanding of laser-matter interaction [15, 16]. The short wavelength (i.e. high photon energy) of ultraviolet (UV) excimer lasers has improved the quality of micromachining and has increased the versatility of features that can be produced using these lasers [4, 16]. UV excimer lasers are effective tools for micromachining and processing of materials with different properties for the following reasons: (i) high absorption of UV wavelengths by most materials makes excimer lasers suitable candidates for processing of transparent materials; (ii) the photon energy is higher than the chemical bond strength in many materials, which improves the efficiency and quality of ablation processes due to minimized thermal effects; (iii) the laser beam can be focused to a spot size smaller than that produced by longer wavelength lasers, all of which improve spatial resolution and extend applications to processing and machining of small features [16].

Several studies have investigated the influence of spot size on ablation rate for various materials using different laser systems [15, 17–20]. Ablation rate of via holes produced on SiC wafers by a 193 nm ArF excimer laser at 100 Hz was found to increase from 0.1 μm/pulse to 0.18 μm/pulse when the hole diameter was decreased from 70 μm to 10 μm [18]. The

authors attributed the increased ablation rate with decreasing hole diameter to the reflected laser light from the side wall of the via hole which is focused on the bottom of the via hole leading to an enhancement of ablation rate [18]. A reduction in ablation rate of polyimide polymers was observed with increasing crater diameter in the fluence range from 2 to 33 J cm^{-2} at excimer laser wavelength of 248 nm [17]. The decrease of ablation rate with spot size was attributed to the attenuation dynamics and plasma shielding of the expanding ablation plume [15, 17, 19]. In plasma shielding, part of the incoming laser pulse energy is lost during interaction with the ablation plume due to scattering, absorption, and reflection processes. The transport of the ablated material, expansion of the plasma plume, and consequently attenuation of the incident laser pulse by the plasma plume, were related to the laser spot size on the sample surface [5, 20, 21]. The ablation plume was assumed to expand over the target surface with a certain angle distribution and a height that depends only on the laser fluence [15]. The amount of ablated material that interacts with the central portion of the incident laser beam is less for smaller spot sizes (i.e. a considerable part of the ablated material is moved outside of the beam area) than larger spot sizes (i.e. the amount of ablated material outside the laser beam is negligible compared to that remaining within the laser beam) [15, 19, 22]. Therefore, the attenuation of the incident laser pulse due to plasma shielding with larger spot sizes is more effective than that with smaller spot sizes [17, 19]. Ablation rate was reported to be independent of laser beam spot size in the case of picosecond or femtosecond laser pulses due to the reduction in or absence of plasma shielding [5, 15, 20, 22].

In this study we investigate the influence of laser beam spot size on ablation rate and amount of material removal from 2024T3 Al alloy in air. A set of craters with spot sizes ranging from 10 to 150 μm were created using an excimer laser operating at a wavelength of 193 nm and at a constant fluence and repetition rate. Three different techniques (LA-ICP-MS, optical and scanning electron microscopy) were used to characterize the ablation process.

2. Experimental

Laser ablation was performed at the University of Windsor, Ontario, Canada using a PhotonMachines laser ablation system (Analyte G2-powered by 193 nm short ATLex 300si excimer laser), which emits radiation at a pulse width less than 4 ns and wavelength of 193 nm. The laser can be operated at a variable repetition rate from 1 to 300 Hz and at a variable energy up to 15 mJ/pulse. The laser energy was controlled by rotating a glass optical attenuation plate positioned in the path of the laser beam. The attenuation plate can be displaced away from the beam path to allow full energy delivery to the sample surface. A set of optical components and an optical homogenizer were used to shape and smooth the laser beam profile to get flat-bottom craters. The laser spot size on the sample surface was varied by imaging a set of apertures of various diameters inserted in the path of the laser beam. The beam was focused on the sample surface using a 16× demagnification objective, which allowed a range of spot sizes from less than 3–160 μm and a maximum fluence of 15 J cm^{-2}. Spot diameters of 10, 20, 40, 85, 110 and 150 μm were investigated in this study. An aluminum alloy (2024-T3 ALCLAD) obtained from Aircraft Spruce and Specialty Company, Ontario, Canada was ablated in a single spot to produce craters of different diameters and varying depths using a variable number of laser pulses delivered at a repetition rate of 20 Hz and a fluence of 11 J cm^{-2}. Samples were cut into pieces of dimensions 2 by 1.5 by 0.3 cm, polished and mounted on a 3D computer-controlled stage (horizontal resolution of 1 μm), where ablation is conducted in air. Ablation rates were determined from the slope of the straight line in the relationship between crater depth and number of laser pulses. Crater depths were measured using an Olympus® BX51 polarizing optical light microscope at 20× and 50× magnifications. Crater morphology was characterized using a FEI Quanta® 200 FEG scanning electron microscope.

3. Results and discussion

3.1. Optical microscopy

Ablation depth of craters was estimated by measuring the difference in z-position between the surface and the bottom of the crater using an optical microscope. Figure 1(A) shows the ablation depth of craters produced at different laser spot diameters as a function of number of laser pulses. Each data point in figure 1(A) represents the average depth of four craters measured at a fluence of 11 J cm^{-2} and a repetition rate of 20 Hz. The variation of ablation rate (calculated from the slopes of figure 1(A)) with laser spot diameter is shown in figure 1(B). Ablation rate was found to decrease from 1.04 μm/pulse at a spot size of 10 μm–0.29 μm/pulse at a spot size of 85 μm. Increasing spot size above 85 μm did not show any further decrease in ablation rate. These results agree with those published by Eyett and Bäuerle [19], which investigated the effect of laser beam spot size of XeCl excimer laser ($\lambda = 308$ nm, pulse width = 11 ns, repetition rate < 10 Hz, and fluence up to 3.1 J cm^{-2}) on the ablation rate of $LiNbO_3$. Eyett and Bäuerle [19] reported a decrease in ablation rate by a factor of approximately 3 with increasing spot size from 24 to 80 μm, followed by saturation for craters with diameters from 80 to 175 μm. A ten-fold increase of ablation efficiency was also reported when decreasing the spot diameter from 220 μm to 9 μm in the fluence range of 7.5 J cm^{-2}–13.2 J cm^{-2} using a KrF nanosecond excimer laser ($\lambda = 248$ nm; pulse width = 20 ns) during percussion drilling through silicon wafer [15].

Experimental and theoretical investigations on the effect of laser beam spot size on the ablation efficiency have attributed the observed decrease in ablation rate with increasing laser beam spot size to the increased attenuation of the incident laser energy for smaller spots by the ablation plume [17, 19]. Beuermann *et al* [22] assumed a linear dependence of ablation rate on the fluence, which is valid in the saturation region above the threshold fluence. They deduced the

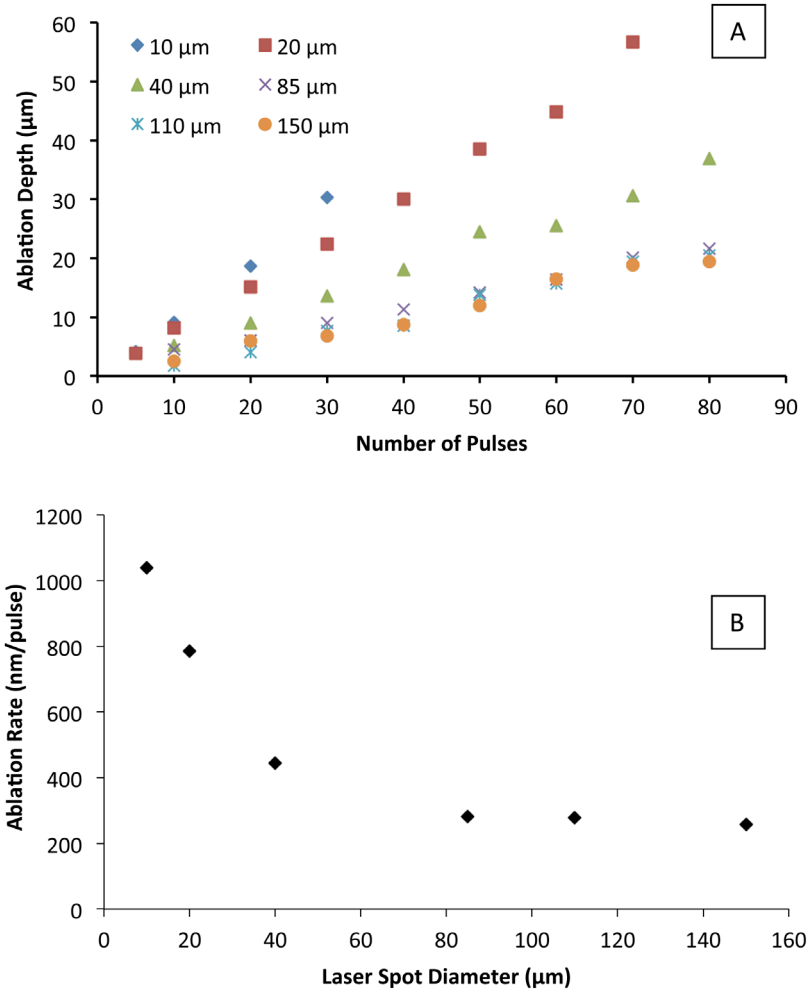

Figure 1. (A) Ablation depth of craters produced at different laser spot size as a function of the number of laser pulses; (B) ablation rate per pulse (as calculated from the slopes of (A) as a function of laser spot diameter. Each data point in (A) represents the average measurement of four crater depths at a fluence of 11 J cm^{-2} and repetition rate of 20 Hz.

following relationship between ablation rate R and laser beam spot radius r [22]

$$R = R_o/\left(1 + \frac{\rho\sigma R_o}{1 + \pi h/2r}\right) \quad (1)$$

where R_o is the ablation rate in the absence of plume attenuation; ρ is the density of the plume; σ is the attenuation coefficient; and h is the distance the ablated particles move during the laser pulse. According to equation (1), a nearly linear relationship between ablation rate R and reciprocal of the spot radius r exists [22] (figure 2). For a very large spot radius, the ablation rate can be expressed by [22]

$$R_\infty = R_o/(1 + \rho\sigma R_o). \quad (2)$$

The dependence of ablation depth on the number of laser pulses for craters produced at different fluence and at a spot size of 35 μm is shown in figure 3. Ablation rate increased from 0.22 μm/pulse at a fluence of 3.04 J cm^{-2}–0.49 μm/pulse at a fluence of 15 J cm^{-2}. Fluence is one of the most important parameters that controls ablation rate and ablation mechanisms. For many materials ablated using laser systems of different properties, ablation rate was found to increase rapidly with increasing fluence at the sample surface until a

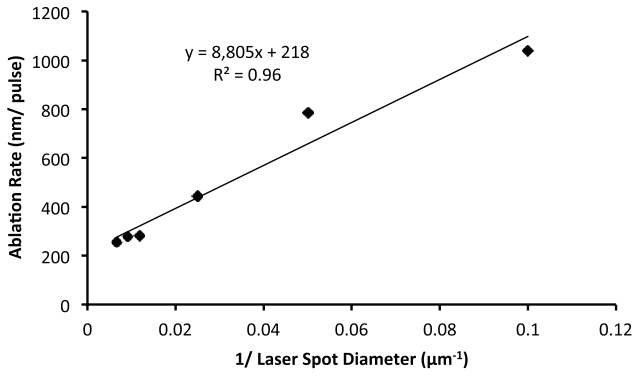

Figure 2. Dependence of ablation rate on the reciprocal of the laser beam spot diameter.

certain value of fluence is reached above which ablation rate saturates or decreases [20, 23–25]. The saturation or decrease in ablation rate at high fluence was linked to the evolution of a plasma plume, which increases the effect of plasma shielding and consequently increases the attenuation of the incident laser energy [20, 23–25]. Ablation at a fluence close to the ablation threshold is generally characterized by low ablation rate and low debris deposition around the crater. In the case of

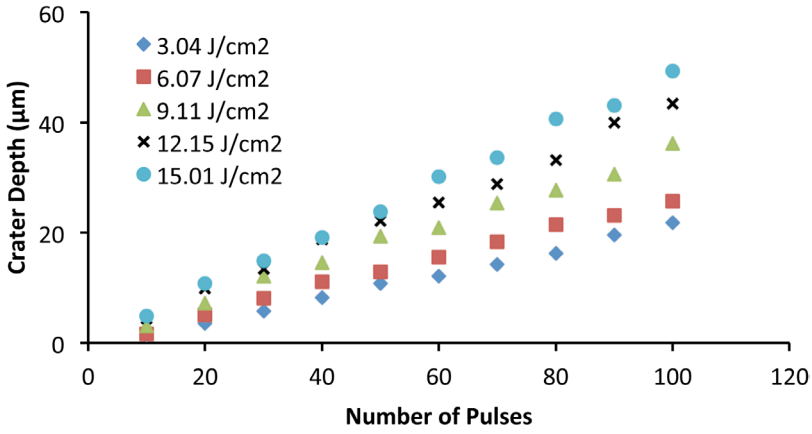

Figure 3. Crater depth as a function of the number of laser pulses at variable fluence. Repetition rate = 20 Hz; laser spot diameter = 35 μm.

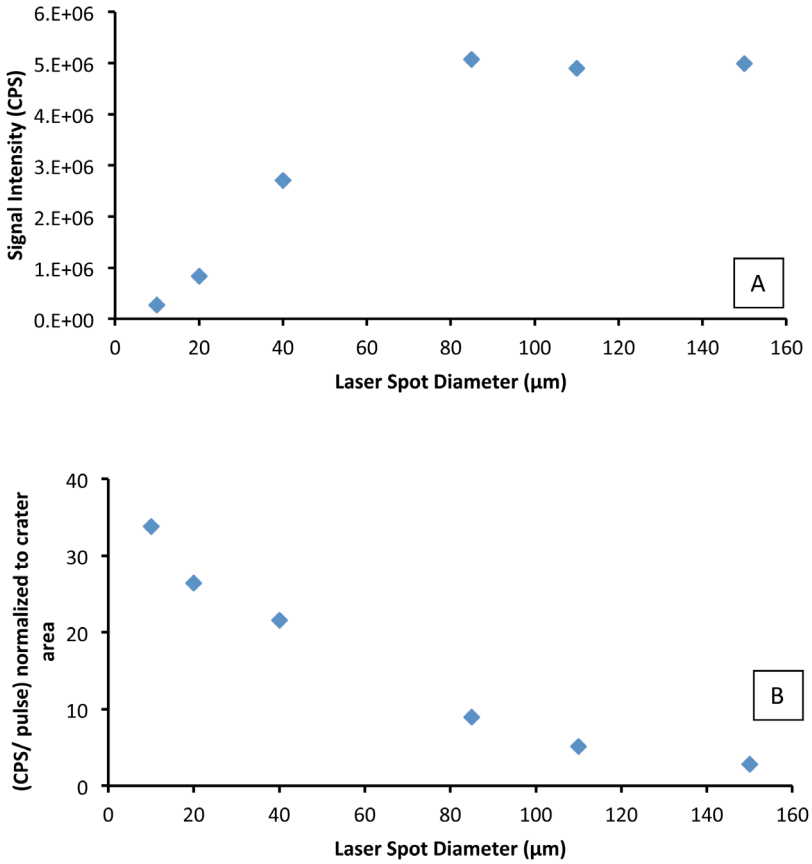

Figure 4. (A) LA-ICP-MS signal intensity as a function of laser spot diameter. Each data point is the average obtained from measurements of four craters. (B) CPS/pulse normalized to crater area as a function of laser spot diameter. The craters were produced by 100 laser pulses at a fluence of 11 J cm^{-2} and a repetition rate of 20 Hz.

femtosecond and short-wavelength nanosecond laser pulses, ablation at low fluence is dominated by non-thermal mechanisms, where melting of the material is not severe. As the fluence increases, thermal ablation mechanisms become more predominant, where melting and ejection of large droplets of molten material are characteristic of the ablation [23, 26].

3.2. LA-ICP-MS

LA-ICP-MS is a quasi-nondestructive technique used for elemental and isotopic analyses of solid samples [27–31]. It is a reliable and sensitive technique for the determination of a wide range of element concentrations (i.e. from ultra trace to percent levels) in solids [29–32]. LA-ICP-MS uses a high power pulsed laser to ablate solid samples located in an air-tight ablation cell. The ablated material is transported from the cell by Ar or He carrier gas through tubing to the mass spectrometer for atomization and ionization by the ion source (i.e. the ICP). The ions are separated and detected inside the mass spectrometer according to their mass to charge ratios. The signal intensity, reported in counts per second (CPS), is proportional to the amount of ablated

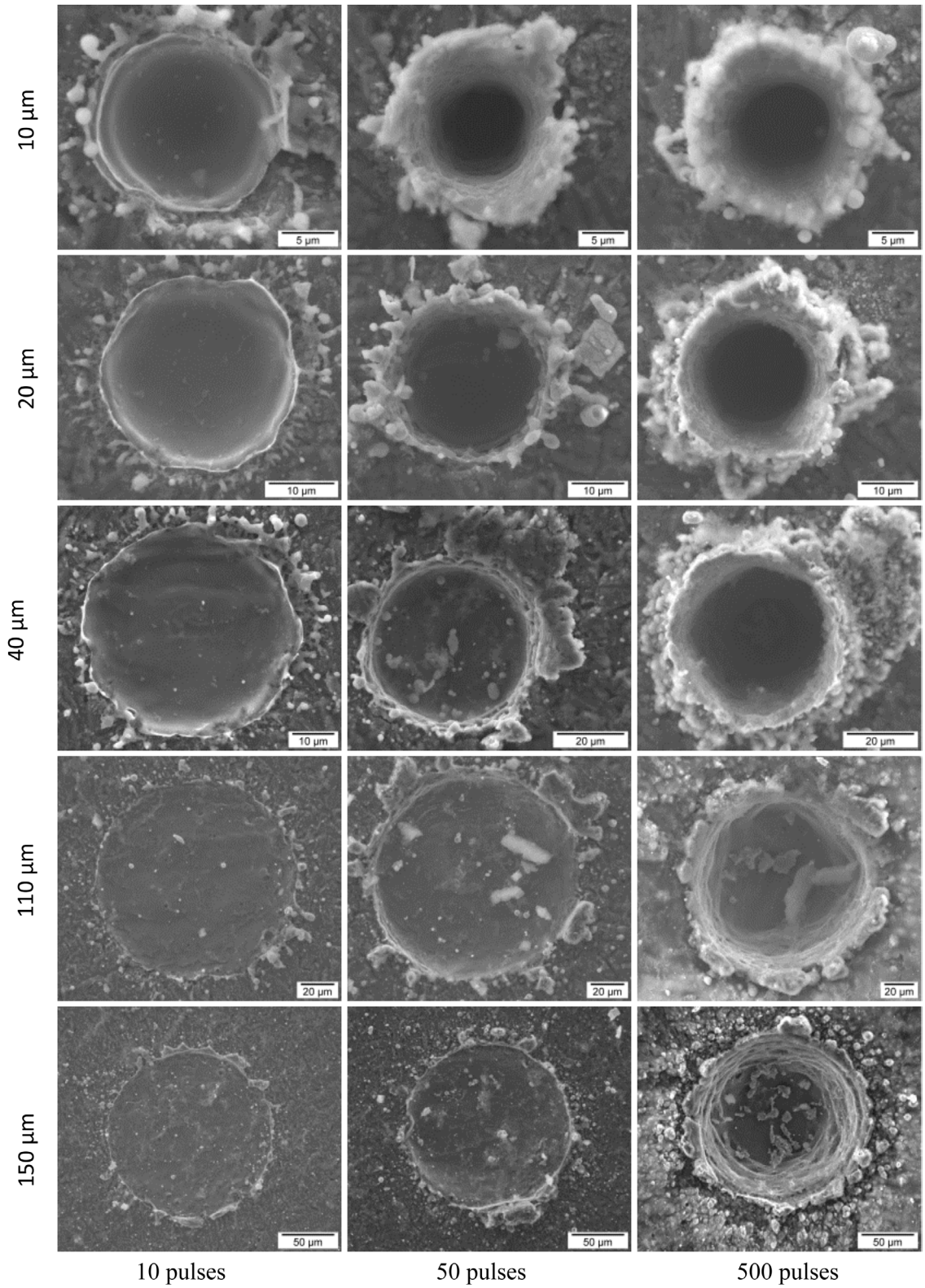

Figure 5. Evolution in morphology of craters produced in air at different laser spot sizes (10–150 μm) and the number of laser pulses (10–500). Fluence and repetition rate were fixed to 11 J cm^{-2} and 20 Hz, respectively.

material that reaches the detector after being atomized and ionized. The concentrations of elements in the unknown solid sample are calculated by comparing the element intensity in the unknowns to that in a standard reference material (i.e. the external calibration standard). In this study, we used LA-ICP-MS as a tool to investigate the effect of laser beam spot size on the amount of ablated material, which is dependent on the crater volume and consequently on the crater depth. This was achieved by using an Agilent 7900 quadrupole ICP-MS for measuring the signal intensity of a major element in the target material (e.g. Al) as a function of laser beam spot diameter.

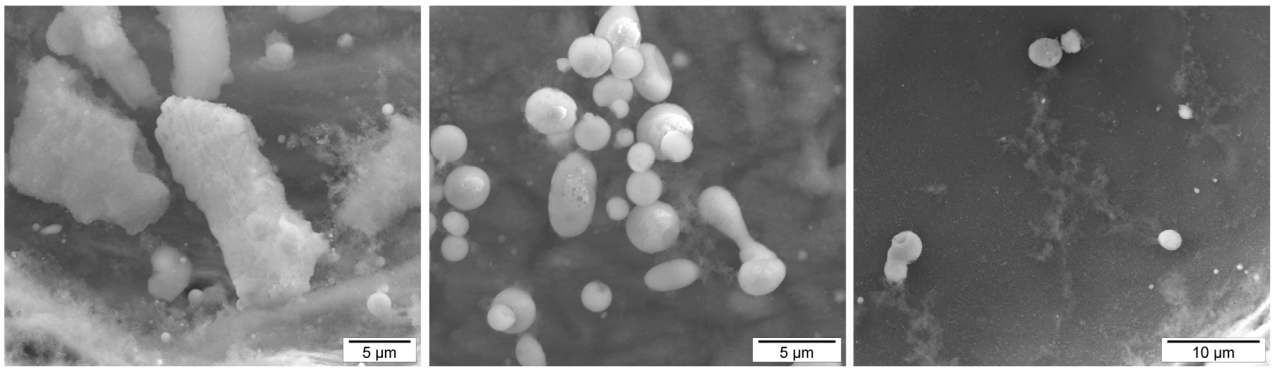

Figure 6. Types of particle seen during excimer laser ablation of Al in air. (A) Large particles formed, most probably, from the collapse of the crater rim; (B) spherical particles formed as a result of melting and ejection of molten material; (C) nanoparticles chains formed as a result of evaporation and condensation.

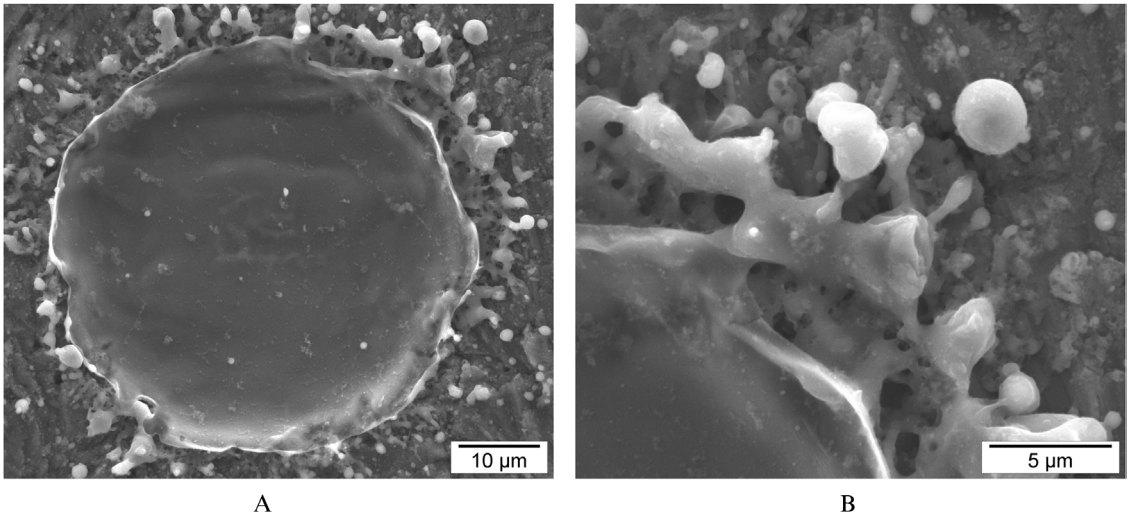

Figure 7. (A) A crater produced by 10 laser pulses at a fluence of 11.02 J cm^{-2}, repetition rate: 20 Hz, and a laser beam diameter: 40 μm. (B) A magnified image at the edge of the crater shown in (A). The signs of melting seen indicate the role thermal processes in material removal.

Figure 4(A) shows the variation of LA-ICP-MS signal intensity of ^{27}Al with laser beam spot diameter for craters produced by 100 laser pulses at a fluence of 11 J cm^{-2} and a repetition rate of 20 Hz. Each data point in figure 4(A) represents the average signal intensity measured for four craters of the same spot diameter. The signal intensity was found to increase rapidly with increasing spot diameter up to 85 μm due to the rapid increase in the crater volume and the amount of ablated material. The signal intensity did not show significant variation at spot diameters greater than 85 μm. This indicates that the amount of ablated material and crater volume became less dependent on the spot diameter for spot sizes greater than 85 μm, which is in agreement with measurements made using optical microscopy.

A crater produced by an excimer laser has a flat-bottom surface and can be approximated by a cylinder of a volume that equals the product of ablation depth and crater area. The dependence of the crater depth on laser beam spot diameter can be obtained from LA-ICP-MS measurements by plotting the average signal intensity per pulse (CPS/pulse) normalized to crater area as a function of laser spot size (figure 4(B)). The area-normalized signal intensity per pulse, which is proportional to the ablation depth/pulse, decreased with laser spot diameter in a similar manner to that observed in the relationship between ablation rate and laser spot size (figure 1(B)). The deviation between figures 1(B) and 4(B) observed for spot sizes greater than 85 μm can be attributed to the following: (i) LA-ICP-MS is a very sensitive technique (~10^6 CPS/ppb for the Agilent 7900), which means that small changes in the amount of ablated material result in large differences in signal intensity; (ii) we assumed that the actual crater area is the same as that of the laser beam spot size, however, there are likely deviations from this assumption due to laser-matter interaction and thermal effects. In general, the behavior of ablation depth with spot diameter is very similar when measured by two different techniques (i.e. optical microscopy and LA-ICP-MS).

3.3. Scanning electron microscopy

Figure 5 shows SEM images of craters ablated by 10, 50, and 500 laser pulses using different laser spot diameters (10, 20, 40, 110, and 150 μm) at a fluence of 11 J cm^{-2} and a repetition rate of 20 Hz. It is clear from the images that the ablation

depth of the craters produced by a fixed number of laser pulses is dependent on the laser beam diameter. This agrees with optical microscopy measurements of the crater ablation depth. It can also be seen from the SEM images that the amount of debris deposited and accumulated around the ablation crater is dependent on the number of laser pulses. Increasing the number of laser pulses leads to an increase in the amount of debris deposition and a build up of a crater rim. A crater rim is formed from re-solidified molten material that cannot escape from the crater. Accumulation and deposition of debris around the craters may be attributed to the inefficient removal of the ablated material and its deposition on the sample surface by the action of gravity due to performing the ablation in ambient atmosphere, where the movement of air molecules is negligible. Conducting ablation in a flowing gas environment or under liquid media reduces or eliminates debris deposition around the crater and leads to a clean crater surface [33–35].

Figure 6 shows different types of particles observed in the ablated products. The first type, shown in figure 6(A), was observed to accompany craters with raised rims. This type of particle (>5 μm in size) most likely originated from the collapse of the crater rim, which led to deposition of structures of different shapes and sizes inside and outside the ablation crater. The second type of particle (figure 6(B)), had spherical shapes and originated from ejection of molten material from the crater onto the surrounding sample surface. The presence of spherical particles and the evidence of melting observed at the crater edge (figure 7) indicate thermal ablation [36–38]. Two types of ablation mechanisms (thermal and non-thermal) can occur during ablation. Both mechanisms can exist simultaneously but to varying degrees depending on the type of material being ablated and the laser properties [39–41]. Thermal (photothermal) ablation is the dominant ablation mechanism in cases of nanosecond long-wavelength laser pulses due to absorption of the incident laser energy by electrons and its subsequent transfer to the lattice during the laser pulse. Thermal ablation depends mainly on thermal conductivity of the target material, fluence, and the laser pulse width [9, 40, 41]. Non-thermal (photochemical) ablation is the dominant mechanism of material removal in cases of ablation using deep ultra violet (DUV) or femtosecond laser pulses [9, 40]. In non-thermal ablation, the absorbed photon energy is directly used to break the chemical bonds, which leads to material removal without thermal effects [9, 40, 41]. Even with femtosecond or nanosecond DUV laser pulses, thermal ablation becomes significant if optimal laser conditions are not applied [9, 23, 26, 40–42].The third type of particle was much smaller in size than the other two types and was characterized by agglomeration into chain-like structures (figure 6(C)). Condensation from the vapor phase is the most probable origin of formation of this type of particle [36, 38, 43, 44].

4. Conclusions

Ablation of Al with nanosecond 193 nm ArF excimer laser in air was investigated using three different techniques. Optical microscopy showed a decrease in ablation rate with increasing the laser beam spot size from 10 to 85 μm. At spot sizes greater than 85 μm, the ablation rate became approximately independent of the laser beam spot size. Similar behavior was observed using LA-ICP-MS measurements from craters produced by 100 laser pulses. The amount of ablated material, which is proportional to crater volume, increased rapidly with increasing laser beam spot size up to 85 μm. A saturation in signal intensity was observed for laser spot diameters greater than 85 μm. Signal intensity per pulse (CPS/pulse) normalized to crater area was found to decrease with increasing laser beam spot size, which indicates a decrease in the amount of ablated material per pulse with increasing laser beam spot diameter. The decrease in ablation rate and amount of ablated material per pulse observed with increasing laser beam spot size is attributed to attenuation of laser energy due to interaction of the incident laser beam with the laser-generated plume. The attenuation of laser energy is less for smaller than larger craters due to the rapid plume expansion and its fast removal from the path of the incident laser beam.

SEM imaging provides excellent qualitative information regarding the products of the ablation process. Surface morphology of craters confirmed the dependence of the amount of ablated material and crater depth on the number of laser pulses and laser beam spot size. The presence of micrometer-sized spherical particles in the ablated material indicates, on one hand, a thermal ablation mechanism where particles are formed from ejected molten material. On the other hand, the formation of nanometer-sized particles, which agglomerate into large chain-like structures, indicates the existence of a non-thermal ablation mechanism. Each mechanism contributes to the ablation process with a degree dependent on target and laser properties (e.g. thermal conductivity, fluence, wavelength, and pulse width).

Acknowledgments

NSERC Discovery Grants to JEG and BJF and CFI/MRI Leading Edge and Leaders Opportunities Funds. The authors would like to thank Sharon Lackie for her help during SEM measurements.

References

[1] Günther D and Heinrich C A 1999 Comparison of the ablation behaviour of 266 nm Nd:YAG and 193 nm ArF excimer lasers for LA-ICP-MS analysis *J. Anal. At. Spectrom.* **14** 1369–74

[2] Günther D, Frischknecht R, Heinrich C A and Kahlert H-J 1997 Capabilities of an argon fluoride 193 nm excimer laser for laser ablation inductively coupled plasma mass spectometry microanalysis of geological materials *J. Anal. At. Spectrom.* **12** 939–44

[3] Delmdahl R and von Oldershausen G 2005 Quantitative solid sample analysis by ArF excimer laser ablation *J. Mol. Struct.* **744–7** 255–8

[4] Bidin N and Ab Razak S N 2012 ArF excimer laser annealing of polycrystalline silicon thin film *Crystallization—Science and Technology* ed M R Barsi Andreeta (Rijeka: InTech) pp 481–506

[5] Bäuerle D 2011 *Laser Processing and Chemistry* (Berlin: Springer)

[6] Bhatt D, Hutt D A and Conway P P 2012 Excimer laser machining of microvias in glass substrates for the manufacture of high density interconnects *Appl. Phys.* B **108** 137–47

[7] Oliveira V, Vilar R and Conde O 1998 Excimer laser ablation of Al_2O_3–TiC ceramics : laser induced modifications of surface topography and structure *Appl. Surf. Sci.* **127–9** 831–6

[8] Heitz J, Pedarnig J D, Bäuerle D and Petzow G 1997 Excimer-laser ablation and micro-patterning of ceramic Si_3N_4 *Appl. Phys.* A **261** 259–61

[9] Liu K, NiCkolov Z, Oh J and 'Moses' Noh H 2012 KrF excimer laser micromachining of MEMS materials: characterization and applications *J. Micromech. Microeng.* **22** 015012

[10] Chang T-C and Molian P A 1999 Excimer pulsed laser ablation of polymers in air and liquids for micromachining applications *J. Manuf. Process.* **1** 1–17

[11] Jelínková H 2013 *Lasers for Medical Applications* (New Delhi: Woodhead)

[12] Siew W O, Yap S S, Ladam C, Dahl Ø, Reenaas T W and Tou T Y 2011 Nanosecond laser ablation and deposition of silicon *Appl. Phys.* A **104** 877–81

[13] Ashfold M N R, Claeyssens F, Fuge G M and Henley S J 2004 Pulsed laser ablation and deposition of thin films *Chem. Soc. Rev.* **33** 23–31

[14] Wang Y L, Chen C, Ding X C, Chu L Z, Deng Z C, Liang W H, Chen J and Fu G S 2011 Nucleation and growth of nanoparticles during pulsed laser deposition in an ambient gas *Laser Part. Beams* **29** 105–11

[15] Brandi F, Burdet N, Carzino R and Diaspro A 2010 Very large spot size effect in nanosecond laser drilling efficiency of silicon *Opt. Express* **18** 23488–94

[16] Ion J C 2005 *Laser Processing of Engineering Materials* (Amsterdam: Elsevier)

[17] Schmidt H, Ihlemann J, Wolff-Rottke B, Luther K and Troe J 1998 Ultraviolet laser ablation of polymers: spot size, pulse duration, and plume attenuation effects explained *J. Appl. Phys.* **83** 5458

[18] Liu L, Chang C Y, Wu W, Pearton S J and Ren F 2011 Circular and rectangular via holes formed in SiC via using ArF based UV excimer laser *Appl. Surf. Sci.* **257** 2303–7

[19] Eyett M and Bäuerle D 1987 Influence of the beam spot size on ablation rates in pulsed-laser processing *Appl. Phys. Lett.* **51** 2054–5

[20] Wolff-Rottke B, Ihlemann J, Schmidt H and Scholl A 1995 Influence of the laser-spot diameter on photo-ablation rates *Appl. Phys.* A **60** 13–7

[21] Heitz J, Wang X Z, Schwab P, Bauerle D and Schultz L 1990 KrF laser-induced ablation and patterning of Y–Ba–Cu–O films *J. Appl. Phys.* **68** 2512–4

[22] Beuermann T, Brinkmann H J, Damm T and Stuke M 1990 Picosecond UV excimer laser ablation of $LiNbO_3$ *MRS Symp. Proc.* vol 191 pp 37–42

[23] Shaheen M E and Fryer B J 2012 Femtosecond laser ablation of brass: a study of surface morphology and ablation rate *Laser Part. Beams* **30** 473–9

[24] Shaheen M E, Gagnon J E and Fryer B J 2014 Femtosecond laser ablation behavior of gold, crystalline silicon, and fused silica: a comparative study *Laser Phys.* **24** 106102

[25] Shaheen M E, Gagnon J E and Fryer B J 2015 Experimental study on 785 nm femtosecond laser ablation of sapphire in air *Laser Phys. Lett.* **12** 066103

[26] Shaheen M E, Gagnon J E and Fryer B J 2013 Laser ablation of iron: a comparison between femtosecond and picosecond laser pulses *J. Appl. Phys.* **114** 083110

[27] Becker J S 2002 State-of-the-art and progress in precise and accurate isotope ratio measurements by ICP-MS and LA-ICP-MS *J. Anal. At. Spectrom.* **17** 1172–85

[28] Pisonero J, Kroslakova I, Günther D and Latkoczy C 2006 Laser ablation inductively coupled plasma mass spectrometry for direct analysis of the spatial distribution of trace elements in metallurgical-grade silicon *Anal. Bioanal. Chem.* **386** 12–20

[29] Koch J and Günther D 2011 Review of the state-of-the-art of laser ablation inductively coupled plasma mass spectrometry *Appl. Spectrosc.* **65** 155A–62A

[30] Hattendorf B and Günther D 2014 Laser ablation inductively coupled plasma mass spectrometry *Handbook of Spectroscopy* ed G Gauglitz and D S Moore (Weinheim: Wiley-VCH) pp 647–97

[31] Shaheen M E, Gagnon J E and Fryer B J 2012 Femtosecond (fs) lasers coupled with modern ICP-MS instruments provide new and improved potential for *in situ* elemental and isotopic analyses in the geosciences *Chem. Geol.* **330–1** 260–73

[32] Albrecht M, Derrey I T, Horn I, Schuth S and Weyer S 2014 Quantification of trace element contents in frozen fluid inclusions by UV-fs-LA-ICP-MS analysis *J. Anal. At. Spectrom.* **29** 1034–41

[33] Shaheen M E, Gagnon J E and Fryer B J 2013 Femtosecond laser ablation of brass in air and liquid media *J. Appl. Phys.* **113** 213106

[34] Chien C Y and Gupta M C 2005 Pulse width effect in ultrafast laser processing of materials *Appl. Phys.* A **81** 1257–63

[35] Kruusing A 2004 Underwater and water-assisted laser processing: part 2—etching, cutting and rarely used methods *Opt. Lasers Eng.* **41** 307–27

[36] Ozawa E, Kawakami Y and Seto T 2001 Formation and size control of tungsten nano particles produced by Nd:YAG laser irradiation *Scr. Mater.* **44** 2279–83

[37] Musaev O R, Midgley A E, Wrobel J M and Kruger M B 2010 Laser ablation of alumina in water *Chem. Phys. Lett.* **487** 81–3

[38] Bogaerts A, Chen Z, Gijbels R and Vertes A 2003 Laser ablation for analytical sampling: what can we learn from modeling? *Spectrochim. Acta* B **58** 1867–93

[39] Chen Y-T, Ma K-J, Tseng A A and Chen P H 2005 Projection ablation of glass-based single and arrayed microstructures using excimer laser *Opt. Laser Technol.* **37** 271–80

[40] Ganeev R A 2014 *Laser Surface Interactions* (Berlin: Springer)

[41] Sohn I-B, Noh Y-C, Choi S-C, Ko D-K, Lee J and Choi Y-J 2008 Femtosecond laser ablation of polypropylene for breathable film *Appl. Surf. Sci.* **254** 4919–24

[42] Le Harzic R, Breitling D, Weikert M, Sommer S, Fohl C, Valette S, Donnet C, Audouard E and Dausinger F 2005 Pulse width and energy influence on laser micromachining of metals in a range of 100 fs–5 ps *Appl. Surf. Sci.* **249** 322–31

[43] Kuhn H-R and Günther D 2005 The agglomeration state of nanosecond laser-generated aerosol particles entering the ICP *Anal. Bioanal. Chem.* **383** 434–41

[44] Hergenröder R 2006 Laser-generated aerosols in laser ablation for inductively coupled plasma spectrometry *Spectrochim. Acta* B **61** 284–300